# Virtual force feedback teleoperation of the InsectBot using optic flow

**Felix Schill⋆ and Robert Mahony⋆ and Peter Corke† and Luke Cole⋆**
⋆ Department of Engineering, Australian National University,
ACT, 0200, AUSTRALIA, {firstname}.{lastname}@anu.edu.au
† CSIRO ICT Centre & Tech., Pullenvale,
Queensland, AUSTRALIA. peter.corke@csiro.au

## Abstract

This paper proposes the use of optical flow from a moving robot to provide force feedback to an operator's joystick to facilitate collision free teleoperation. Optic flow is measured by a pair of wide angle cameras on board the vehicle and used to generate a *virtual* environmental force that is reflected to the user through the joystick, as well as feeding back into the control of the vehicle. We show that the proposed control is dissipative and prevents the vehicle colliding with the environment as well as providing the operator with a natural feel for the remote environment. Experimental results are provided on the InsectBot holonomic vehicle platform.

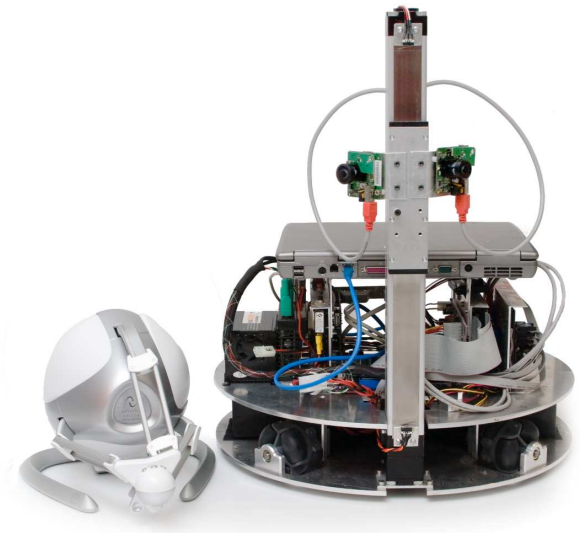

Figure 1: The InsectBot and the Falcon 3D haptic device.

## 1 INTRODUCTION

Bilateral force feedback teleoperation is a field that has its roots in the 1940's with the construction of the first remotely controlled robotic manipulator. The character of the modern subject was set in the eighties with the introduction of energy-based analysis [1], passivity-based control design [2], and scattering theory [3]. More recent work provided a geometric setting for scattering theory [4]. Many of the key breakthroughs in the field have been associated with overcoming the destabilising effects of variable time-delays and packet switched data in the communications channel and this has driven much of the research in the last decade [5; 6; 7; 8; 9; 10] A recent review paper [11] provides an excellent overview of the field. Teleoperation of mobile vehicles is itself an active field of research with work on improving the human machine interface to mobile platforms [12], improved autonomy and path planning of vehicles [13]. Bilateral force feedback teleoperation of a mobile vehicle was considered in [14] where the vehicle bumpers were equipped with force sensing strain gauges. More typically, however, it is not desirable that a mobile vehicle physically contacts its environment and that a haptic telepresence be based on virtual forces derived from exteroreceptive sensors mounted on the vehicle. Several authors have proposed to generate haptic force based on artificial force fields derived from sensors such as ultrasonic or laser scanners along with environment mapping techniques [15; 16; 17; 18]. Optic flow in the image space is coupled to time-to-collision computations [19] and has been proposed as a sensor modality for obstacle avoidance [20; 21], docking manoeuvres [22; 23; 24; 25], and visual odometry [26]. To the authors knowledge, there has been no prior work that has used optic flow motion cues as a sensor modality for haptic telepresence.

In this paper, we propose the use of haptic feedback to the remote operator of a mobile vehicle based on optic flow measured by a vision system mounted on the vehicle. The optic flow measures used are spherical op-

tical divergence computed at the focus of expansion and a comparative flow difference computed at the equatorial points relative to the focus of expansion. A similar approach was proposed earlier by Coombs [21]. Force derived from the spherical divergence motion cue provides the operator with a feel for an impending collision, pushing back against the joystick with force inversely proportional to time-to-contact. Force derived from the comparative flow difference acts orthogonally to the main motion of the robot, and guides the operator to control the vehicle to move down the centre of corridors and minimise the chance of side-swipe collisions without opposing the forward motion of the vehicle.

The vehicle is modelled as a dynamic system, with virtual dynamic state and direct kinematic control of the vehicle velocity. Within this framework the haptic forces generated by the optic flow are also applied as virtual forces to the vehicle dynamics. This adds collision avoidance and corridor centring capability directly to the mobile vehicle irrespective of input from the operator. The proposed algorithm has been implemented on the InsectBot developed at ANU/NICTA. The vision system consists of two firewire cameras with wide angle 190° lenses that provide near complete visual coverage of the local environment of the robot. The force feedback is implemented on low-cost haptic device designed for gaming (see fig. 1). The resulting system provides good feel for the operator and enables significantly improved remote operation of the vehicle.

After the introduction, §2 introduces the system model considered. Section 2 introduces a bond graph model of the coupled teleoperation system. The key new component of this system is the environmental impedance that is discussion in Section 3. Implementation details and experimental results are provided in Sections 4 and 5.

## 2 System Model

In this section, a model of the system is introduced using the bond graph syntax to demonstrate the flow of energy in the system. The virtual force due to the environment is modelled as an impedance.

Consider the bond graph model shown in Figure 2. The upper dashed box in Figure 2 represents the haptic subsystem. The flow source $S_f$ at the far left is the user force input to the haptic joystick. This model represents the fact that a pilot will feel the force reflected by the system, however, these forces will be sufficiently small that, apart form a small compliance of the hand (modelled as a spring impedance $Z_{\text{hand}}$), they will not effect how the pilot positions the joystick. Velocity of the joystick, $\dot{\xi}$, coupled with force, $f$, is modelled as power into the dynamics of the haptic joystick. The force feedback from the vehicle is modelled as a modulated source of effort, again supplying power to the joystick. The dynamics of

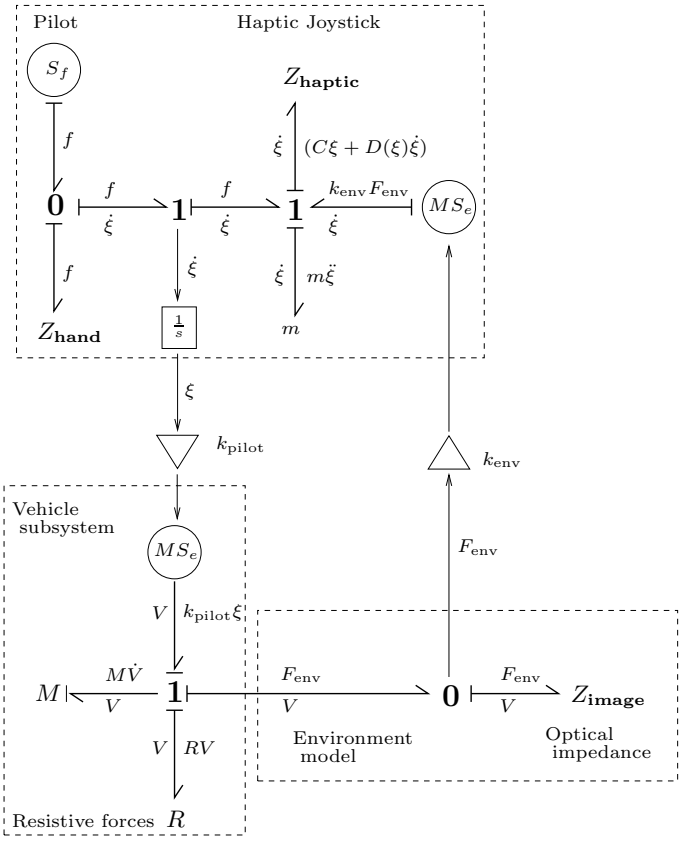


Figure 2: Bond graph formulation of system model.

the haptic joystick are modelled by the 1-junction with damping and spring impedance $Z_{\text{haptic}}$ generating a force $C\xi + D(\xi)\dot{\xi}$ and an inertia $m$ generating the inertial force $m\ddot{\xi}$. The resulting dynamics of the haptic subsystem are

$$m\ddot{\xi} = C\xi - D(\xi)\dot{\xi} + f + k_{\text{env}}F_{\text{env}} \tag{1}$$

The damping $D(\xi)$ for low-end haptic device can be quite significant and is unknown. In contrast, the spring impedance $C > 0$ is added by the algorithm to provide a centring force on the haptic joystick so that the operator is always aware of applying force to the vehicle. The offset of the joystick is used as the control input for the vehicle dynamics. Using the syntax of bond graphs a 1-junction is used to obtain the velocity $\dot{\xi}$ that is then integrated to obtain $\xi$. In practice, the value $\xi$ is available directly from the haptic joystick.

The dashed box on the lower left of Figure 2 denotes the two degree-of-freedom vehicle translation dynamics. The modulated effort source $MS_e$ at the top of this box denotes the virtual force demanded by the operator while the 1-junction combines the reflected environmental forces $F_{\text{env}}$ with a resistive damping term $R$ and the

virtual inertial term $M$. The resulting vehicle dynamics are

$$M\dot{V} = -\Omega \times V - RV + k_{\text{pilot}}\xi + F_{\text{env}} \tag{2}$$

where $\Omega$ is the rotational velocity of the vehicle and the velocity $V$ is expressed in the body-fixed-frame. The angular dynamics are not modelled and are controlled separately as a kinematic demand by the operator. The angular velocity of the system is taken as an exogenous input to the virtual vehicle dynamics (2).

The dynamic model (2) is simulated with inputs from the environmental force and the joystick. The velocity states of the model are used as control demands for the robot platform. This introduces a natural low pass filtering (that can be tuned by choosing the virtual vehicle's mass $M$) of the operator's demand to the vehicle control which is highly desirable in practice.

The final subsystem (lower right dashed box Figure 2) represents the interaction of the vehicle with the environment through the observed image sequence. The 0-junction is simply a notational convention to extract the signal $F_{\text{env}}$. The key to modelling this subsystem is understanding the way in which optic flow can be used to generate a force that will be reflected both to the operator and directly into the vehicle control system. We model this bond as an impedance, that is a mapping that accepts a velocity and returns a force. Since we will use a vision system to define the impedance we will term this an *optical impedance*.

## 3 Optical Impedance

In this section, we define an optical impedance based on two optical motion cues in order to define the environmental impedance $Z_{\text{env}}$ in Figure 2.

Assume that the environment and illumination in which the vehicle moves is static. We will assume that the camera system used is fully calibrated and pixel coordinates have been mapped onto the sphere to model a spherical camera. The spherical optic flow is defined as the instantaneous observed velocity of image features on the surface of the sphere. Denote coordinates on the spherical image surface by vectors $p \in S^2$, the sphere $S^2 = \{p \in \mathbb{R}^3 \mid |p| = 1\}$. We denote the optic flow field by $\Phi_t(p)$, where $t$ is the frame (or time) index and $p$ is the pixel coordinates, defined on the image plane. The optical flow observed in a particular direction depends on the distance to the environment in that direction as well as the velocity of the robot. Let $\lambda_t : S^2 \to \mathbb{R}$ denote a scalar field on the sphere, defined at frame $t$, with values denoting the distance from the focal point of the camera to the environment. The spherical optic flow $\Phi_t$ is given by [27]

$$\Phi(p) := -\Omega \times p - \frac{1}{\lambda(p)}\left(I_{3\times 3} - pp^\top\right) V \tag{3}$$

where $I$ is the $3 \times 3$ identity matrix and $(V, \Omega)$ is the velocity of the robot and hence the camera. The dependence of the optic flow on the inverse depth to the observed environment is a key property of optic flow that underlies previous applications to obstacle avoidance and docking manoeuvres [21; 23; 25].

We consider an optical impedance generated by two complementary motion cues similar to those used by Coombs *et al.* [21].

The spherical divergence of the optical flow $\Phi$ is given by

$$\text{div}\Phi(p) = \frac{2p^\top V}{\lambda(p)} + \frac{d\lambda(p)\cdot\Phi(p)}{\lambda(p)} \tag{4}$$

Note that the optic flow $\Phi_t$ is zero in the direction of motion of the vehicle. That is

$$\Phi_t\left(\frac{V}{|V|}\right) = 0$$

The direction of motion can be computed from a wide angle measurement of the optic flow of the vehicle [28]. The direction of motion of the vehicle can also be directly measured by computing the focus of expansion of the translation optic flow

$$\Phi_t^{\text{trans}}(p) = \Phi_t(p) + \Omega \times p = -\frac{1}{\lambda(p)}\left(I - pp^\top\right) V$$

That is the part of the optic flow that is associated with the translation of the vehicle independent of its rotation. Given that the angular velocity is measured accurately from kinematic odometry this calculation is sufficiently accurate to produce a good estimate of the translational optic flow field.

Define an optical motion cue

$$w_{\text{foe}} = \begin{cases} \text{div}\Phi(V/|V|) & \text{for } V \neq 0 \\ 0 & \text{for } V = 0 \end{cases}$$

where 'foe' stands for focus of expansion. The direction $V/|V|$ is computed as the focus-of-expansion of the translational optic flow field $\Phi_t^{\text{trans}}$. Since the divergence of full flow does not depend on the rotation, the optical motion cue $w_{\text{foe}}$ is also the the divergence at the focus of expansion of the translational optic flow field. The focus-of-expansion of the translational flow is not defined for $V = 0$, however, the motion cue $w_{\text{foe}}$ remains well defined since the limit

$$\lim_{V\to 0} \text{div}\Phi(p) = 0$$

regardless of the direction $p$ taken.

Define the equatorial circle

$$E_{\text{diff}} := \{p \in S^2 \mid \langle p, V\rangle = 0\}.$$

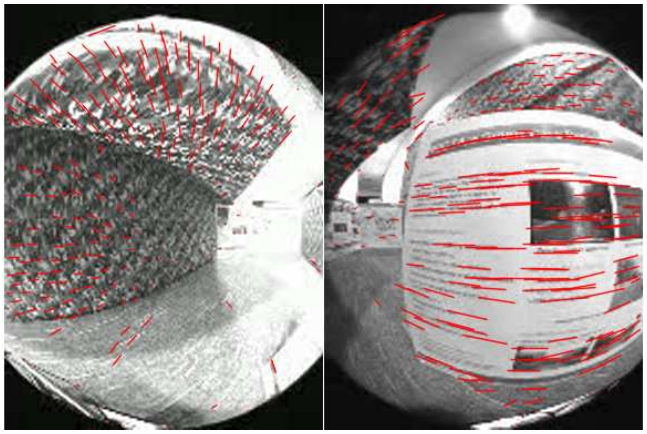

Figure 3: Optical flow vectors, displayed with the raw camera images of the left and right camera.

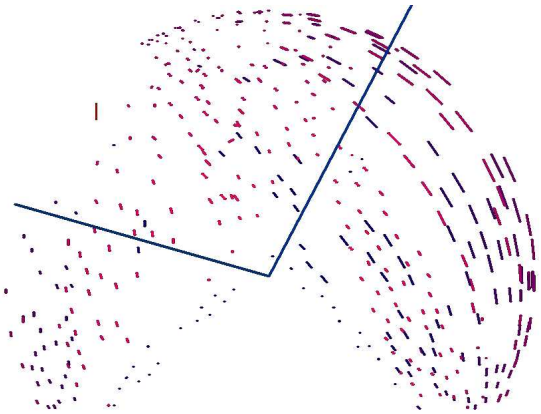

Figure 4: Spherical mapping of the flow field. Also shown are the direction of travel (black, pointing to the left) and the (inverse) equatorial force $-\omega_{\text{diff}}$ (blue).

Note that $E_{\text{diff}}$ is well defined as a circle for $V \neq 0$ while for $V = 0$ one has $E_{\text{diff}} = S^2$. Define an optical motion cue by

$$w_{\text{diff}} := \begin{cases} \int_{E_{\text{diff}}} \langle \Phi_{\text{trans}}(p_\theta), V \rangle \, p_\theta d\theta & \text{for } V \neq 0 \\ 0 & \text{for } V = 0 \end{cases}$$

where (for $V \neq 0$) the circle $E_{\text{diff}}$ is parameterised by the angle $\theta$ and $p_\theta$ denotes the $S^2$ coordinates of the parameter. The optical motion cue $w_{\text{diff}}$ compares the component of translational optic flow in the direction of motion at antipodal points orthogonal to the direction of motion.

Based on the two optical motion cues $w_{\text{foe}}$ and $w_{\text{diff}}$ we define the environmental force to the optical impedance to be

$$F_{\text{env}} := \begin{cases} -\left( c_{\text{foe}} w_{\text{foe}} \frac{V}{|V|} + c_{\text{diff}} w_{\text{diff}} \right) & \text{for } V \neq 0 \\ 0 & \text{for } V = 0 \end{cases}$$

where $c_{\text{foe}}, c_{\text{diff}} > 0$ are positive constants.

The choice of environmental force in this way has an important energy flow interpretation. The (virtual) power or energy flowing into (or out of) the environmental impedance $Z_{\text{env}}$ is given by the product of the conjugate variables $F_{\text{env}}$ and $V$. Thus the power of the environmental impedance is given by

$$\begin{aligned} \langle V, F_{\text{env}} \rangle &= - c_{\text{foe}} w_{\text{foe}} V^\top \frac{V}{|V|} + c_{\text{diff}} V^\top w_{\text{diff}} \\ &= - c_{\text{foe}} \text{div}\Phi \left( \frac{V}{|V|} \right) |V| \\ &\quad + \int_{E_{\text{diff}}} \langle \Phi_{\text{trans}}(p_\theta), V \rangle \left( V^\top p_\theta \right) d\theta \\ &= - 2 c_{\text{foe}} \frac{|V|^2}{\lambda (V/|V|)} \end{aligned}$$

where the differential term contributes zero power since $\left(V^\top p_\theta\right) = 0$ for $p_\theta$ taken in orthogonal to the focus-of-expansion. Thus, since $\lambda > 0$ is always positive the optical impedance proposed is dissipative, that is, energy is always lost through the environment bond. As a consequence the environment acts as a resistive stabilising term in the system dynamics. Indeed, the energy dissipation in the environmental impedance is inversely proportional to the distance to the environment along the direction of motion. As a consequence, any trajectory that actually collides with the environment would dissipate infinite virtual energy in the limit as the collision occurs. Since the only source of energy entering the system is the bounded power demanded by the operator it is clear that the vehicle should never collide with the environment. This desirable property is due to the spherical divergence term in the optical impedance. The differential optic flow term is a passive impedance, that is it does not induce a power flow. In practice, this corresponds to forces that help guide the vehicle without opposing or augmenting force input from the pilot.

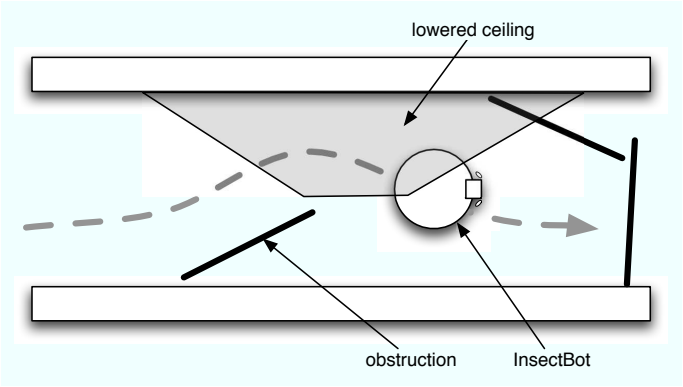


Figure 5: Sketch of the corridor which was used for the first experiment.

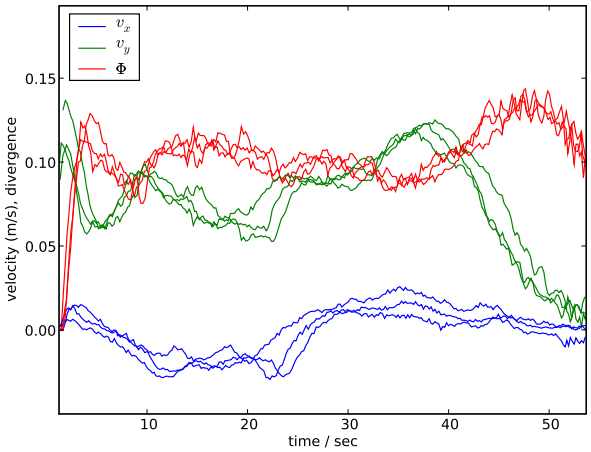


Figure 6: Robot velocity and divergence from three trials in the same environment.

## 4 Implementation

We implemented the algorithm described above on the InsectBot (fig. 1), a holonomic wheeled robot. The InsectBot carries two digital video cameras mounted on a linear lift system. The cameras can therefore freely move in 4 dimensions, namely horizontal translation ($x$ and $y$), vertical translation ($z$), and rotation $\omega_z$ around the $z$-axis. The wheels have closed-loop velocity control, the lift platform is absolute-position controlled. To unify the dynamics of the vehicle, and to approximate the dynamics of a hovering platform, virtual dynamics are computed based on (2). The resulting 3-D velocities (or position for the $z$-axis) are applied to the wheels and the lift platform.

The cameras are equipped with fisheye lenses with 190° field of view (Omnitech Robotics lens). Due to image plane limits, the field of view is around 190° vertically and 180° horizontally. For the following experiments, the two cameras are mounted with the optical axis parallel to the ground plane, pointing 45° left and right of the forward direction. The total field of view is therefore roughly 270° horizontally, with a 90° blind spot backwards.

Sparse optical flow is computed on the planar camera images using a pyramidal implementation of the Lukas and Kanade algorithm. The resulting sparse 2-D vectorfields are mapped onto a spherical representation, while taking camera calibration into account. The 3-D spherical vectorfield is a good approximation of optical flow on a single spherical camera. All following calculations of divergence and flow cues are performed in 3-D on the spherical field.

The optical flow cues are calculated as described in section 3, but with one difference to accomodate the sparse, rather than continuous, vector fields on the sphere. Instead of calculating divergence only in the focus of expansion, divergence is calculated by convolution of the flow field with a derivative-of-Gaussian filter around the focus of expansion. Similarly, equatorial flow $\omega_{\text{diff}}$ is integrated over a Gaussian-filtered environment around the equator:

$$w_{\text{diff}} := \int_{S^2} \langle \Phi(p_\theta), V \rangle \cdot g(\langle p_\theta, V \rangle) p_\theta d\theta$$

with $g(x) := e^{-x^2/\sigma^2}$. By chosing $\sigma$ appropriately, vectors ahead and behind the current robot position (along the direction of travel) can be taken into account. This preemptively steers the robot away from approaching obstacles, and prevents clipping obstacles that are just behind the equator. For the experiments a fairly large value of $\sigma_E = 0.4$ was chosen for equatorial flow, and $\sigma_f = 0.25$ for frontal divergence (relative to the unit sphere).

## 5 Experimental results

The experiments were carried out in a 1.5 m wide corridor (fig. 5). Additional obstacles were added to force the robot to drive in an "S"-curve, first to the left, then to the right and finally stop in front of a blockage. The walls are covered with textured fabric to simulate a well-textured outdoor environment.

The first experiment investigates the behaviour of the robot in a cluttered environment, given a constant forward acceleration command. The operator is assumed to be uncooperative, i.e. the joystick is fixed in the forward position and does not move. The robot maintains a constant orientation during the experiment. The purpose of this experiment is to show the robustness of the system against operator errors. Results of three independent runs with the same starting position are shown in figure 6.

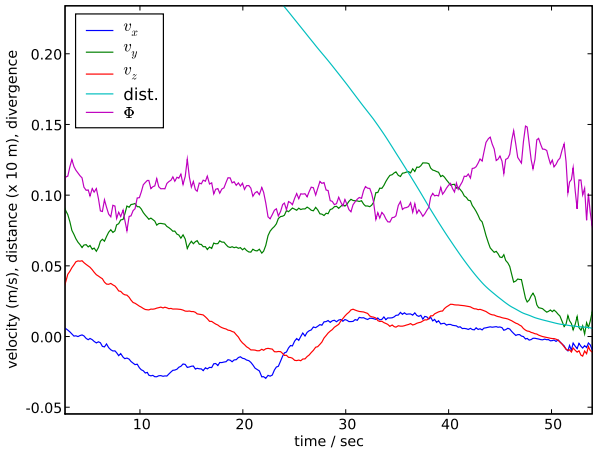


Figure 7: Velocity in $x$ and $y$ and frontal divergence from the corridor experiment. As the robot approaches the rear wall, forward velocity decreases to (almost) zero.

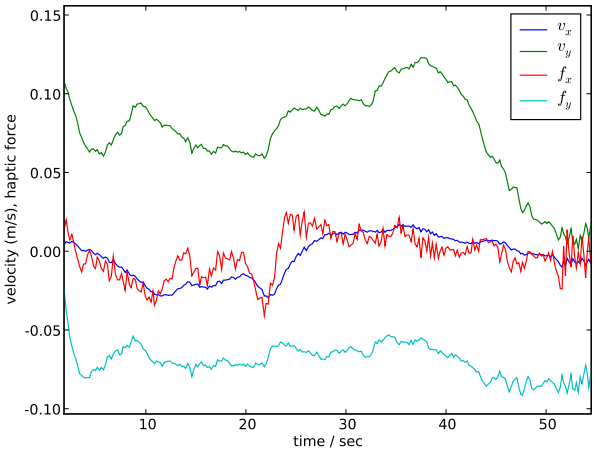


Figure 8: Velocity and haptic force applied to the haptic control device.

Figure 7 shows the lateral velocity $v_x$, the forward velocity $v_y$ and the frontal divergence as measured in the current direction of travel (which is not necessarily the forward direction of the robot). The robot avoids the lateral obstacles (as can be seen by the progression of $v_x$) while maintaining forward speed. As it gets closer to the obstruction at the end of the corridor ($t$=40 sec), the forward velocity decreases as a result of the resisting force from the measured frontal divergence. The robot eventually stops in front of the obstruction. Figure 8 shows the force applied as haptic feedback. As the operator is not responding to applied forces, the stick position does not change. However, the haptic force increases during the approach of the obstruction.

In the second experiment the joystick was allowed to move while being controlled by a human operator. The joystick position is determined by the human control input and the force applied to the joystick by the optical flow system. The results are shown in figures 9 and 10. The results from figure 9 show the response of the system, as the operator gives short forward commands, moving the robot towards a wall, and then lets go of the control stick. It can be seen that the repelling force caused by frontal divergence builds up against the operator's hand. The stick immediately moves backwards as the operator lets go (i.e. $t = 71$, $t = 80$, etc.), and the forward velocity sharply drops. As there is no obstruction behind the robot, the velocity actually becomes negative, increasing the distance to the potential obstacle. It has to be noted that this particular behaviour (overshoot of the joystick) deviates slightly from the theoretical case, and is caused by mechanical imperfections of the haptic device, and time lags present in the system. It does however not affect the overall safety of the system. It can be seen i.e. at $t = 83$ and $t = 93$ that the haptic force decreases, and the joystick returns to the center position, once the robot stops approaching the obstacle. During the successive approaches to the wall, the robot gets closer and closer to the obstruction. The plot shows clearly that the divergence $\Phi$ (shown in red) increases, while the velocity $v_y$ (shown in green) remains roughly the same, or even increases slightly. Likewise, the perceived haptic force increases as well as the distance to the wall becomes smaller. The experiment demonstrates the behaviour of the system in a "panic" situation where the operator lets go of the controls. An impending collision is successfully avoided. Furthermore, increasing haptic forces on the joystick give a clear warning signal to the operator that the robot is approaching an obstacle.

Figure 10 shows a scenario where the robot is within 10-20 centimeters of a potential collision with the wall, as the operator intentionally tries to drive forward into the obstruction. Despite the constant forward-accelerating joystick input $j_y$, the velocity drops as divergence and repelling force on the haptic device increase rapidly. Eventually the operator gives in to the resisting force on the joystick, and despite a few more pushes forward, the collision is avoided.

Further preliminary experiments include driving along the corridor from the first experiment without any visual feedback for the operator. The operator was able to drive the robot through the corridor while avoiding collisions by purely relying on haptic input. However, no formal investigation of the operator experience was conducted yet. Improving the

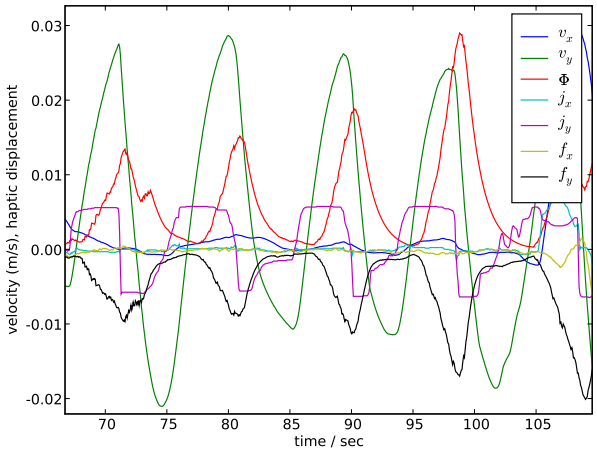


Figure 9: The repelling force ($f_y$) increases for the same velocity and stick input, as the robot gets closer to a planar obstruction.

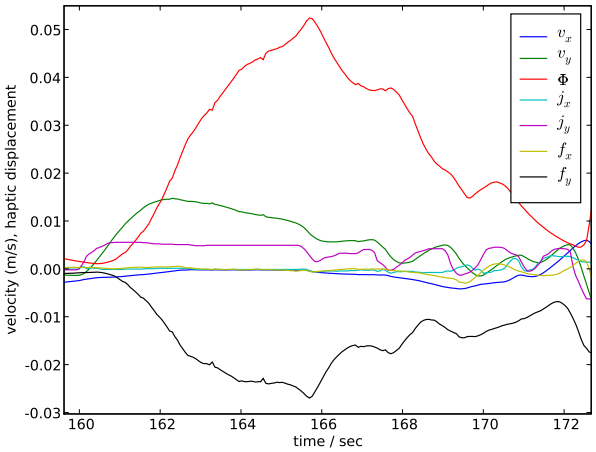


Figure 10: As the robot gets extremely close to the obstruction, the forward velocity $v_y$ decreases despite a constant forward command from the joystick $j_y$. At the same time, the repelling force on the joystick pushes against the operator with increasing force.

haptic experience for the operator is subject of future work. A video of the preliminary trials is included with this paper (see conference proceedings CD, or `http://research.scinamics.com/videos/acra08.m4v`)

## 6 CONCLUSIONS AND FUTURE WORK

We have proposed the use of spherical optical flow from a moving robot to provide force feedback to an operator's joystick to facilitate collision free teleoperation. The spherical optical flow is approximated by flow computed from two onboard wide-angle cameras and mapped to the sphere in order to implement the control law. A dynamic model of a virtual vehicle provides a unifying framework to combine operator demands and environmental force derived from optical flow. The environmental force is also reflected to the user through forces applied to the joystick. We have also shown that the proposed control is dissipative and prevents the vehicle colliding with the environment.

Experimental results on a planar robot with a lift-platform are a precursor to experiments on a flying platform. We are currently commissioning a small-scale quad-rotor hovering vehicle for this purpose.

## Acknowledgments

The authors thanks Jonathan Oh for many discussions on the nature of optical impedance as well as much of the code for the Falcon 3D force feedback joystick. We would also like to thank Nick Barnes at NICTA for providing the InsectBot for the experiments.

## References

[1] N. Hogan, "Impedance control: An approach to manipulation," *Journal of Dynamic Systems, Measurement and Control*, vol. 109, pp. 1–24, 1985. Parts I, II, III.

[2] G. Niemeyer and J. Slotine, "Stable adaptive teleoperation," *IEEE Journal on Oceanic Engineering*, vol. 16, pp. 152–162, Jan. 1991.

[3] R. Anderson and M. Spong, "Bilateral control of teleoperators with time delay," *IEEE Transactions on Automatic Control*, vol. 34, pp. 494–501, May 1989.

[4] S. Stramigioli, A. van der Schaft, B. Maschke, and C. Melchiorri, "Geometric scattering in robotic telemanipulation," *IEEE Transactions on Robotics and Automation*, vol. 18, pp. 588–596, Aug. 2002.

[5] K. Kosuge, H. Murayama, and K. Takeo, "Bilateral feedback control of telemanipulators via computer network," in *Proceedings of the IEEE/RSJ international conference on intelligent robots and systems*, vol. 3, p. 13801385, 1996.

[6] G. Niemeyer and J.-J. Slotine, "Using wave variables for system analysis and robot control," in *Proceedings of the IEEE international conference on robotics and automation*, vol. 3, (Albuquerque, NM, USA.), pp. 1619–1625, 1997.

[7] G. Niemeyer and J.-J. Slotine, "Towards force-reflecting teleoperation over the internet," in *Pro-*

*ceedings of the IEEE international conference on robotics and automation*, vol. 3, pp. 1909–1915, 1998.

[8] Y. Yokokohji, T. Imaida, and T. Yoshikawa, "Bilateral control with energy balance monitoring under time-varying communication delay," in *In Proceedings of the IEEE international conference on robotics and automation*, vol. 3, (San Francisco, CA, USAs), pp. 2684–2689, 2000.

[9] J.-H. Ryu, D.-S. Kwon, and B. Hannaford, "Stable teleoperation with time-domain passivity control," *IEEE Transactions on Robotics and Automation*, vol. 20, no. 2, pp. 365–373, 2004.

[10] S. Stramigioli, C. Secchi, A. van der Schaft, and C. Fantuzzi, "Sampled data systems passivity and discrete port-hamiltonian systems," *IEEE Transactions on Robotics*, vol. 21, pp. 574–587, Aug. 2005.

[11] P. F. Hokayem and M. W. Spong, "Bilateral teleoperation: An historical survey," *Automatica*, vol. 42, pp. 2035–2057, December 2006.

[12] K. Schilling and H. Roth, "Control interfaces for teleoperated mobile robots," in *Proc. 7th IEEE International Conference on Emerging Technologies and Factory Automation ETFA '99*, vol. 2, pp. 1399–1403, 18–21 Oct. 1999.

[13] T. Makiishi and H. Noborio, "Sensor-based path-planning of multiple mobile robots to overcome large transmission delays in teleoperation," in *Proc. IEEE International Conference on Systems, Man, and Cybernetics IEEE SMC '99*, vol. 4, pp. 656–661, 12–15 Oct. 1999.

[14] O. J. Rösch, K. Schilling, and H. Roth, "Haptic interfaces for the remote control of mobile robots," *Control Engineering Practice*, vol. 10, no. 11, pp. 1309–1313., 2002.

[15] S.-G. Hong, J.-J. Lee, and S. Kim, "Generating artificial force for feedback control of teleoperated mobile robots," in *Proceedings of the IEEE/RSJ international conference on intelligent robots and systems*, vol. 3, pp. 1721–1726, 1999.

[16] N. Diolaiti and C. Melchiorri, "Teleoperation of a mobile robot through haptic feedback," in *Proc. IEEE International Workshop 2002 HAVE Haptic Virtual Environments and Their Applications*, pp. 67–72, 17–18 Nov. 2002.

[17] J. Lim, J. Ko, and J. Lee, "Internet-based teleoperation of a mobile robot with force-reflection," in *Proc. IEEE Conference on Control Applications CCA 2003*, vol. 1, pp. 680–685, 23–25 June 2003.

[18] U. W. Boschloo, T. M. Lam, M. Mulder, and M. M. van Paassen, "Collision avoidance for a remotely-operated helicopter using haptic feedback," in *IEEE International Conference on Systems, Man and Cybernetics*, 2004.

[19] D. Lee, "A theorey of visual control of braking based on information about time to collision," *Perception*, vol. 5, no. 4, pp. 437–459, 1976.

[20] R. Nelson and J. Aloimonos, "Obstacle avoidance using flow field divergence," *IEEE Transactions on Pattern Analysis and Machine Intelligence*, vol. 11, no. 10, pp. 1102–1106, 1989.

[21] D. Coombs, M. Herman, T. Hong, and M. Nashman, "Real-time obstacle avoidance using central flow divergence and peripheral flow," *IEEE Transactions on Robotics and Automation*, vol. 14, no. 1, pp. 49–59, 1998.

[22] P. Questa, E. Grossmann, and G. Sandini, "Camera self orientation and docking manouevre using normal flow," in *Proceedings of SPIE - the International Society for Optical Engineering*, vol. 2488, (Orlando), pp. 274–283, 1995.

[23] J. Santos-Victor and G. Sandini, "Visual behaviours for docking," *Computer Vision and Image Understanding*, vol. 67, pp. 223–238, September 1997.

[24] C. McCarthy and N. Barnes, "Performance of optical flow techniques for indoor navigation with a mobile robot," in *Proceedings of the IEEE International Conference on Robotics and Automation*, pp. 5093–5098, 2004.

[25] C. McCarthy, N. Barnes, and R. Mahony, "A robust docking strategy for a mobile robot using flow field divergence," *IEEE Transactions on Robotics*, to appear. Accepted for publication March 2008. (Available online DOI=10.1109/TRO.2008.926871).

[26] M. Srinivasan, J. Chahl, K. Weber, S. Venkatesh, M. Nagle, and S. Zhang, "Robot navigation inspired by principles of insect vision," *Robotics and Autonomous Systems*, vol. 26, pp. 203–216, 1999.

[27] T. Hamel and R. Mahony, "Visual servoing of an under-actuated dynamic rigid-body system: An image based approach.," *IEEE Transactions on Robotics and Automation*, vol. 18, pp. 187–198, April 2002.

[28] J. Lim and N. Barnes, "Directions of egomotion from antipodal points," in *Proceedings of CVPR*, 2008.